Supporting Information for

On the effects of hyperpolarized water-based dissolution on the solute and solvent ^{1}H NMR spectra of small molecules

Dmitrii Aleshin*, Korin Butbul, Itai Hahami, Daniel Abergel and Lucio Frydman*

Department of Chemical and Biological Physics, Weizmann Institute of Science, Rehovot 7610001, Israel

Supporting Section S1: Water's signal during dissolution – Origins and applied corrections

The frequency of the water signal was here assumed given by the sum of a temperature-dependent chemical shift and a hyperpolarization-dependent demagnetizing-field contribution:

$$\delta\nu = \nu(T) + \nu(DF) \quad \text{S1}$$

These demagnetization and temperature induced frequency shift contributions were here estimated as follows:

Demagnetizing field correction. Larmor frequency shift due to the demagnetization field for a uniformly magnetized cylinder with magnetization M_0 is given by[1]:

$$\Delta\nu = \frac{1}{3}\mu_0\gamma M_0 \quad \text{S2}$$

Consider thus the nuclear ^{1}H paramagnetism of a pure water sample under Boltzmann equilibrium at 11.7 T and 300 K. The ensuing magnetization is M_0 = 0.038 A/m, leading to a nuclear paramagnetic field strength $\mu_0\gamma M_0/3 \sim 0.7$ Hz. Under HyperW condition this value increase by 40 – 50 times. In all our HyperW experiments the solute resonances exhibited approximately constant initial frequency shifts of about 40 Hz (t = 0.6 s., enhancement = 1040), which decreased progressively as water hyperpolarization decayed. Under the assumption that the demagnetization field scales linearly with the instantaneous water polarization, the time-dependent demagnetizing shift was modeled as:

$$\nu(t) = \nu_{DF}\frac{Hyper\,(t)}{Hyper(0.6\,s.)} \quad \text{S3}$$

where *Hyper*(t) is the time-dependent water hyperpolarization, and *Hyper*(0.6 s) is the enhancement in the second of the acquired post-dissolution spectra, which occurring ca. 0.6 s after the water's arrival into the NMR tube was our first stable 1D acquisition. The prefactor ν_{DF} was the experimentally observed initial demagnetization field shifts of the solute signals in each dissolution; e.g., 41 Hz for Figure 1 and 44 Hz for Figure 2. The ensuing prediction of the demagnetization field shifts are further illustrated in Figure S1.

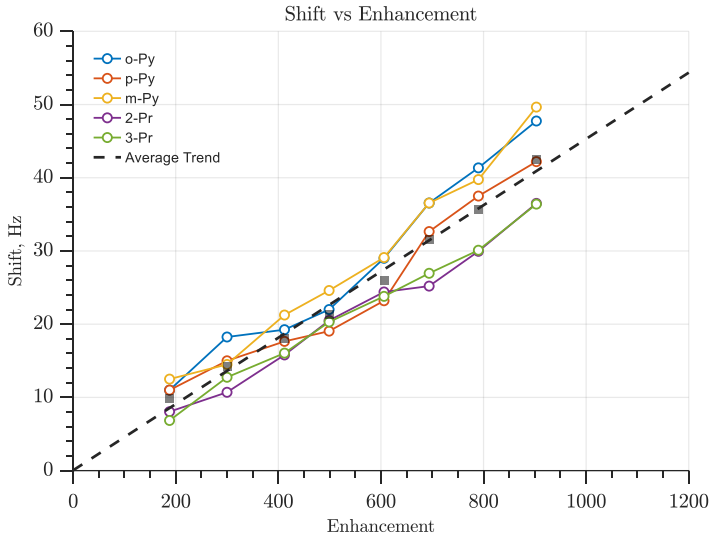

Figure S1 DF-induced shift vs dead-time corrected water enhancements (Fig. 4) affecting the solute's chemical shifts for sample I. Each point represents shifts and water enhancement for the same post-dissolution time point.

Notice that despite the different water enhancements for sample I and sample II, their ν_{DF} values end up approximately identical. We ascribe this behavior to differences in the effective proton concentration prior to dissolution, that reduces observed enhancement while keeping magnetization and related demagnetization field constant. In particular, the 150 µL of 1 M Alanine solution contained an additional amount of non-polarized water which was introduced for pH adjustment, leading to an enhanced DF.

Temperature correction. A small but potentially relevant shift in the peaks also arose because of the cooling undergone by a hyperpolarized water sample reaching the NMR at ca. 40 ˚C, being injected into an NMR tube at ca. 25 ˚C. These temperature variations were accounted for by combining the known temperature dependence of water's chemical shift[2], with a simple heat-transfer model describing thermal equilibration of the sample after dissolution. The latter sample temperature equilibration was modeled as

$$T(t) = T_\infty + (T(0) - T_\infty) * e^{-\frac{t}{\tau}} \quad \text{S4}$$

where T(0) is water's temperature at the time of dissolution, T_∞ is ambient temperature, and τ is the characteristic thermal relaxation time. Based on such temperature change, the time-dependent water resonance frequency shift was calculated as:

$$\nu = 500 * \left(4.96 - o1p - 0.0111 * T(t)\right) \quad \text{S5}$$

where the prefactor 500 corresponds to 1 ppm at our ^{1}H Larmor frequency, o1p was the transmitter offset in ppm, and T(t) is expressed in °C. Figure S2 shows how this equation fitted an actual "dummy" dissolution of a water sample that has not been hyperpolarized, yet passed the same

thermal history as a HyperW dissolution sample. For all samples, a thermal relaxation time $\tau = 24$ s and an ambient temperature $T_\infty = 25$ °C fit well the data; initial temperatures were taken between 35 °C and 40 °C depending the injection. All experiments confirmed that the slow residual water frequency drift observed at longer times is consistent with such thermal re-equilibration.

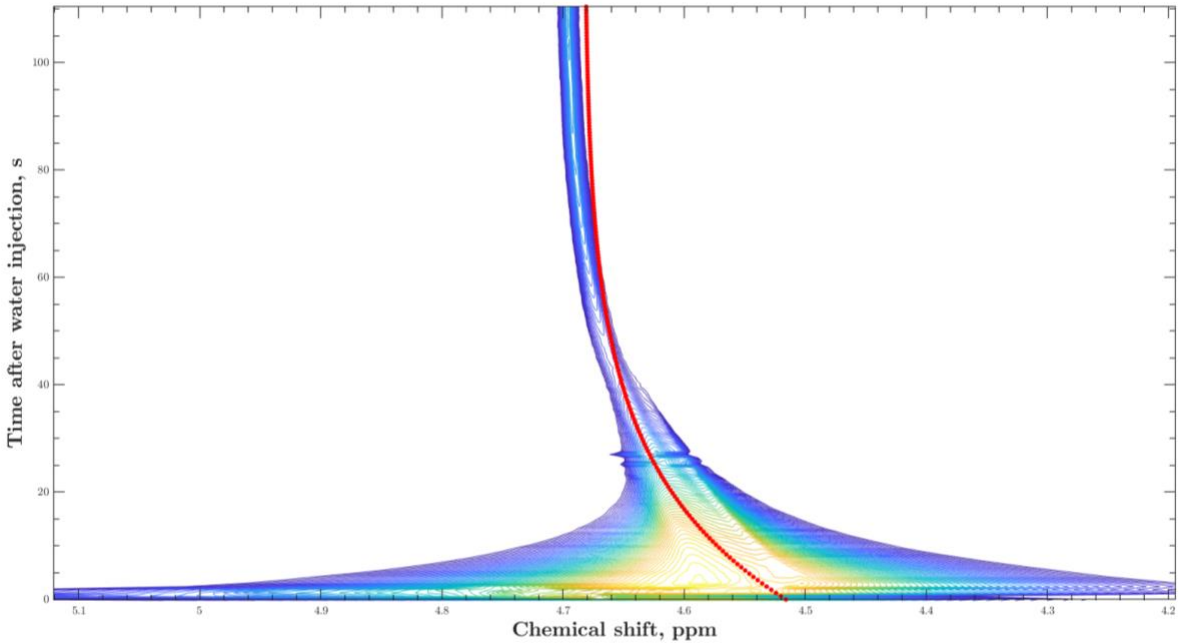

Figure S2: Experimental spectra for dummy sample. Red points reflects exploited water chemical shift dependence with $\tau = 24$ s and initial temperature 40 °C.

Supporting Section S2: Additional experimental and simulation details

All simulations were performed assuming a constant detuning angle ψ. Magnetization enhancements and radiation-damping parameter $|\lambda_{RD}|$ were allowed to vary with post-dissolution time. The spectrometer dead time (10 μs) was explicitly included in all simulations; without this correction simulations required an apparent linear *increase* of the $|\lambda_{RD}|$ with respect water enhancement, reflecting the loss of the early FID points under strong radiation-damping conditions. Even with these provisions, we observed that during an initial post-dissolution period ($t \leq 10$ s) the radiation-damping parameter $|\lambda_{RD}|$ still increased slightly with time, converging for $t > 10$ s to a steady, constant value (Fig. S3). This small, ≤3% change could be traced to the transient change that the probe quality factor Q and the probe resonance frequency ω_{LC}, underwent upon injection of hyperpolarized water. This in turn was a result of variations in the dielectric properties of the sample and of the NMR tube filling (Fig. S4). In particular, the observed increases in the real and imaginary parts of the dielectric permittivity ε' and ε'' at higher temperatures will lead to enhanced dielectric losses and to a reduction of Q –qualitatively consistent with the observed time dependence of $|\lambda_{RD}|$. In view of this, the temporal evolution of the radiation-damping parameter obtained from simulations was also modeled phenomenologically as:

$$|\lambda_{RD}(t)| = \lambda_0(t) + \Delta\lambda_{RD}(1 - e^{-\frac{t}{\tau}}) \quad \text{S6}$$

where λ_0 is the initial value immediately after dissolution, $\Delta\lambda_{rd}$ is the amplitude of the transient change, and τ is the characteristic equilibration time (Fig. S3).

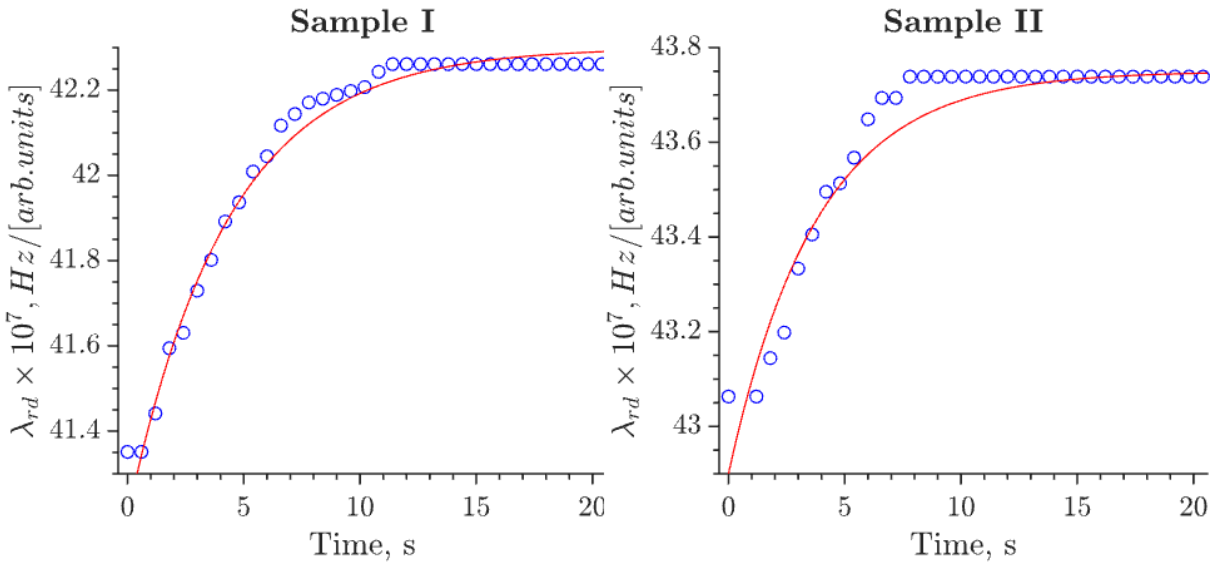

Figure S3: Left λ_{rd} time dependence for sample I. $\lambda_0 = 41.2\times10^{-7}$, $\Delta\lambda_{rd} = 1.1\times10^{-7}$, $\tau = 4.3$ s. Right λ_{rd} time dependence for sample II. $\lambda_0 = 42.9\times10^{-7}$, $\Delta\lambda_{rd} = 0.85\times10^{-7}$, $\tau = 3.8$ s.

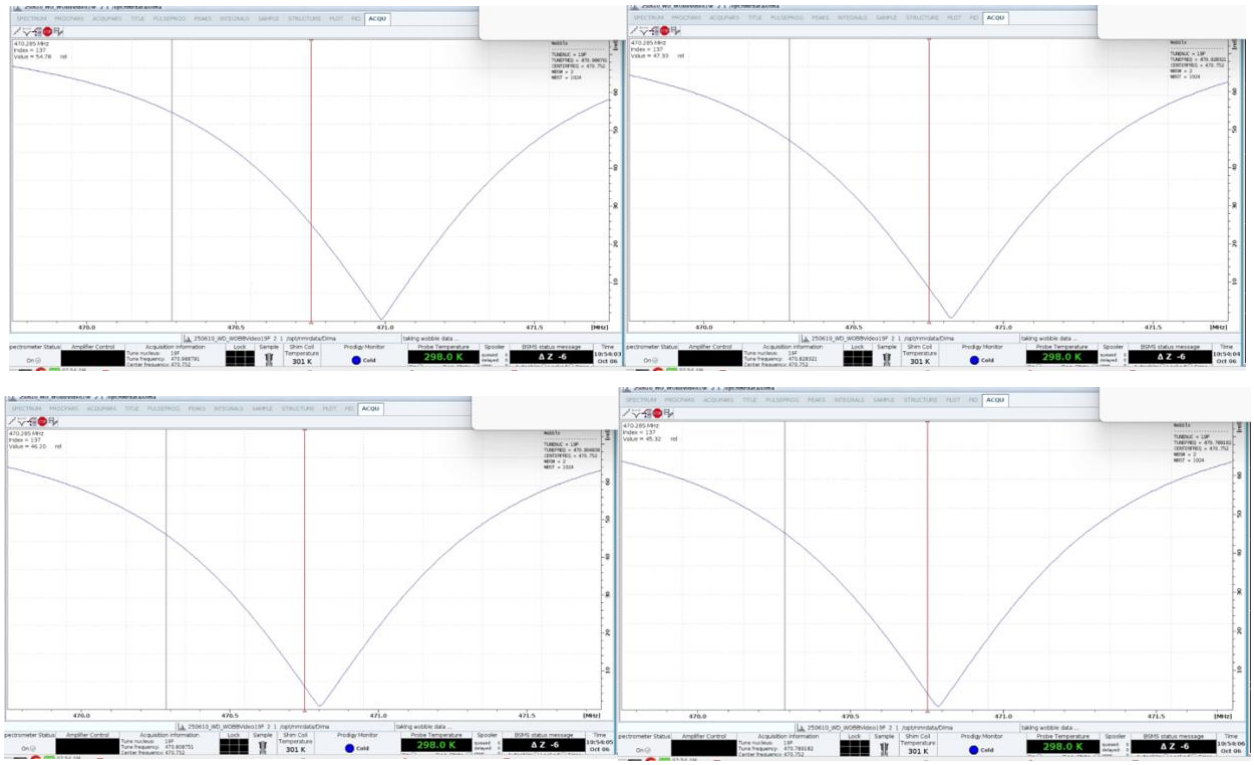

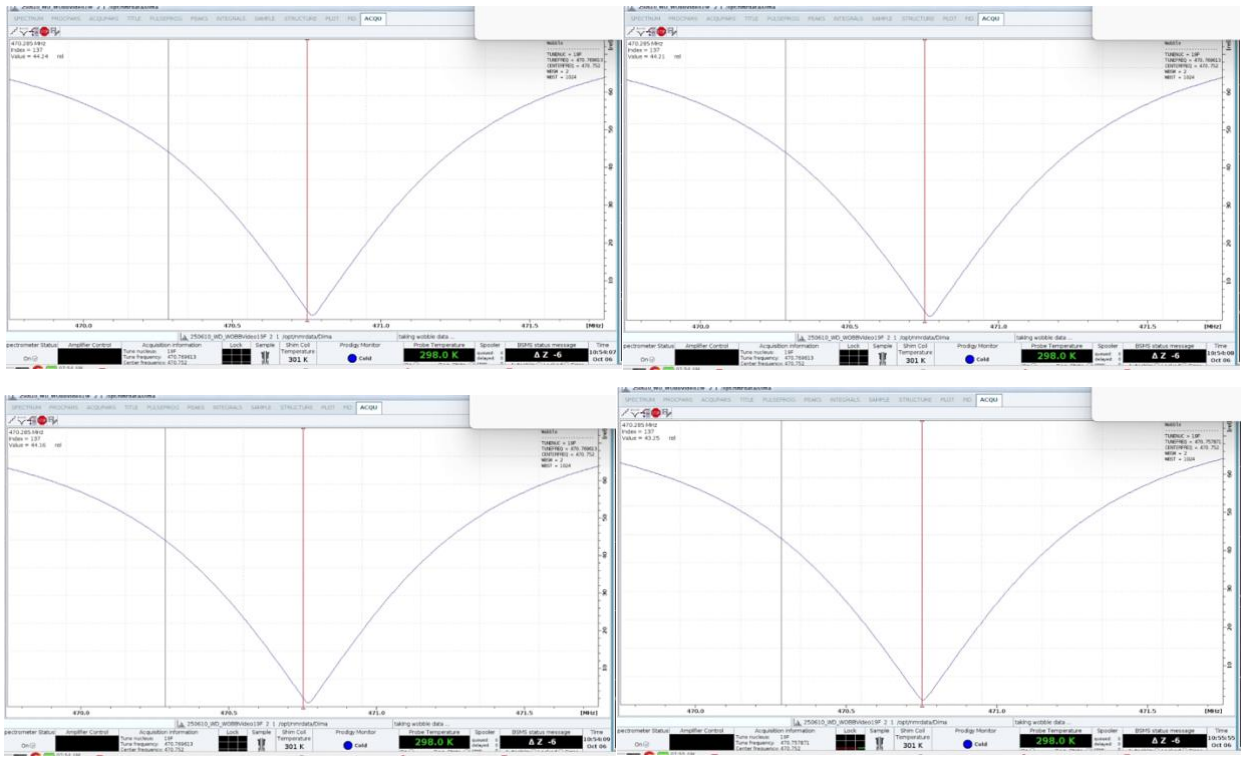

Figure S4: Snapshots of the ^{19}F reflection curve during a hyperpolarized water dissolution, starting from the top left and moving towards the bottom right with one-second spacings. The last snapshot (bottom right) presents the reflection curve 2 minutes after the injection.

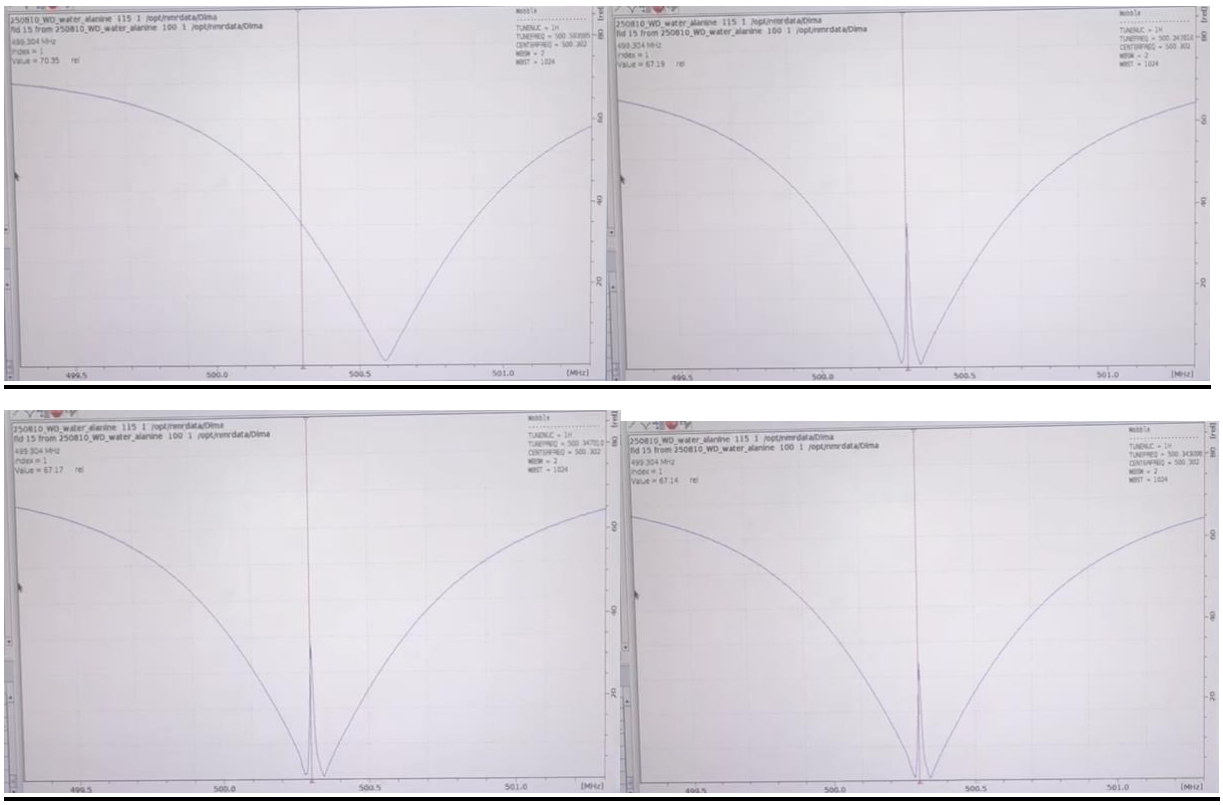

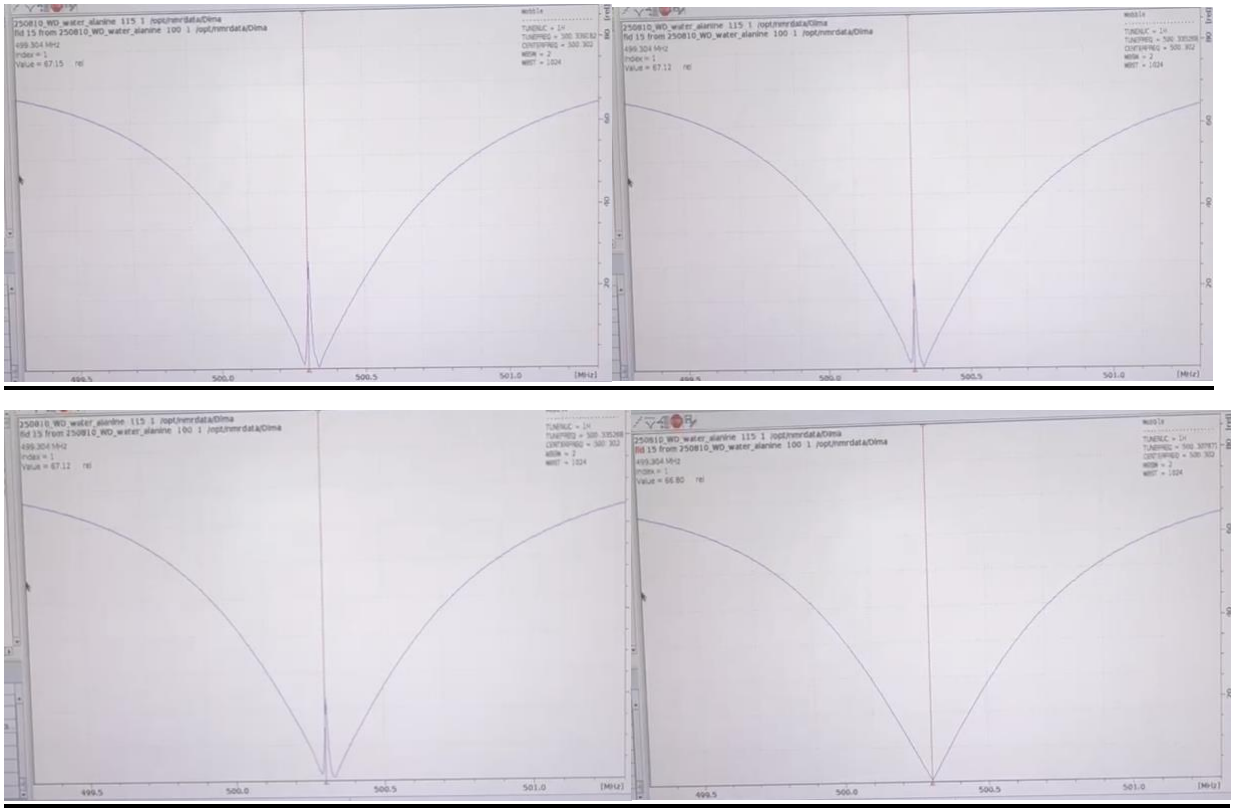

Figure S5: Snapshots of the ^{1}H reflection curve during a hyperpolarized water dissolution, starting from the top left and moving towards the bottom right with one-second spacings. The last snapshot (bottom right) presents the reflection curve 1.5 minutes after the injection.

Supporting videos V1 and V2 uploaded with this document, illustrate the continuous post-dissolution changes in these reflection curves.

Supporting Section S3: Solute enhancements and exchange kinetic fits

Numerical simulations. All spectra were processed using in-house MATLAB scripts. Solute signal intensities were obtained by integrating the absolute value of the spectral signal relative to a locally defined baseline that accounted for the overlapping water. Baselines were determined individually for each resonance by a linear function, with slopes determined by spectral regions located at ±100-150 Hz for the NH signal and ±80-100 Hz for all other resonances –always around a manually-assigned solute signal center. Simulations incorporated water enhancements corrected for instrumental dead time, while solute magnetizations were normalized relative to the thermal equilibrium water integral and corrected with inverse factor (Eq. 12) during the first 20 s, when the water linewidth is significant and RD influence is significant (|A| factor deviates significantly from unity, when R_{rd} and $\Delta\omega$ are the same order):

$$M_j = \frac{I_j}{I_{H_2O,0}} \qquad \text{S7}$$

Cross-relaxation and chemical exchange processes were analyzed using Solomon equations augmented to include chemical exchange terms; to this end the time evolution of each solute's magnetization was described by

$$\dot{M}_i = -\left(R_{ij} + \sigma_{ij}\right)\left(M_j - M_j^0\right) + k_{ij}M_j \quad \text{S8}$$

where R_{ij} and σ_{ij} denote the longitudinal relaxation and cross-relaxation matrices, respectively, and k_{ij} represents the chemical exchange matrix. σ_{ij} included only intermolecular NOE contributions between hyperpolarized water and solute spins, and was constructed as

$$\sigma_{ij} = \sigma_i n_j^i \quad \text{S9}$$

where n_j^i is the number of equivalent protons at site j of the solute molecule i and σ_i is the intermolecular NOE rate constant per proton between water and molecule i. The chemical exchange constants ratio was determined from the thermal NMR signal integrals, according to the principle of mass conservation

$$\frac{k_{ij}}{k_{ji}} = \frac{I_{i,0}}{I_{j,0}} \quad \text{S10}$$

where k_{ij} is exchange constants from site j to site i. $I_{j,0}$ and $I_{i,0}$ – thermal integrals of the site j and i respectively. Tables S1 and S2 describe the best-fit parameters that resulted from such analyses.

Table. S1 Dissolution simulation parameters for the case of Figure 1.

Site	T_1, s	$\sigma\times10^{-4}$, s^{-1}	$n_{s,a}$
3-Pr	4.5	0.5	3
2-Pr	5.3		2
o-Py	7.8	1.8	2
p-Py	7.8		1
m-Py	7.4	2.16	2
H_2O	8.6	-	-

Table. S2 Simulation parameters for dissolution experiment of the case of Figure 2.

Site	T_1, s	$I_{H2O,0}/ I_{x,0}$	$\sigma\times10^{-4}$, s^{-1}	k_{ex}, s^{-1}	n_i
NH	0.4	254	-	17.4	-
Me	1.5	-	1.1	-	3
H_2O	7.8	1	-	-	-

CEST experiments. To complement the data shown in Table S2, CEST experiments were performed using the same dissolution sample. The NH resonance was selectively irradiated in

these experiments using continuous-wave RF irradiation with power P = 10^{-4} W for saturation times between 0 and 6 s. To analyze the ensuing data a saturation efficiency of 1 was assumed, and the equilibrium intensity ratio was defined as

$$f = \frac{I^0_{H_2O}}{I^0_{NH}} = 200 \qquad \text{S10}$$

The intensity of the water signal under NH saturation was described by[3]:

$$I(t) = I_0\left(\frac{T_{ex}}{T_1+T_{ex}} + \left(1 - \frac{T_{ex}}{T_1+T_{ex}}\right)e^{-t\frac{T_1+T_{ex}}{T_1 T_{ex}}}\right) \qquad \text{S11}$$

where T_1 is the longitudinal relaxation time of water and $T_{ex} = f/k_{ex}$ is the exchange time constant. Figure S6 shows the results obtained, together with a best fit and ensuing parameters

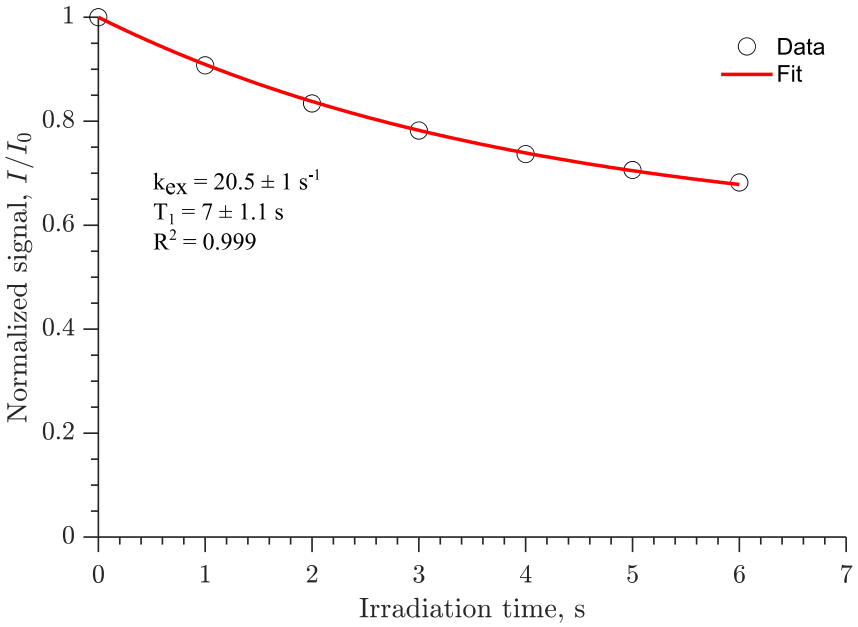

Figure S6: Water signal intensity ratio as a function of NH irradiation time in a control CEST experiment, leading to parameters closely matching those arising from the HyperW experiments.

Literature

1 M. H. Levitt, Demagnetization field effects in two-dimensional solution NMR, *Concepts in Magnetic Resonance*, 1996, **8**, 77–103.

2 H. E. Gottlieb, V. Kotlyar and A. Nudelman, NMR Chemical Shifts of Common Laboratory Solvents as Trace Impurities, *J. Org. Chem.*, 1997, **62**, 7512–7515.

3 J. Zhou and P. C. M. V. Zijl, Chemical exchange saturation transfer imaging and spectroscopy, *Progress in Nuclear Magnetic Resonance Spectroscopy*, 2006, **48**, 109–136.